Data-Driven Regression of Thermodynamic Models in Entropic Form

Matteo Pini(✉), Andrea Giuffre', Alessandro Cappiello, Matteo Majer, and Evert Bunschoten

Propulsion and Power, Delft University of Technology, Delft, The Netherlands
m.pini@tudelft.nl

Abstract. Modeling non-ideal compressible flows in the context of computational fluid-dynamics (CFD) requires the calculation of thermodynamic state properties at each step of the iterative solution process. To this purpose, the use of a built-in fundamental equation of state (EoS) in entropic form, i.e., $s = s(e, \rho)$, can be particularly cost-effective, as all state properties can be explicitly calculated from the conservative variables of the flow solver. This approach can be especially advantageous for massively parallel computations, in which look-up table (LuT) methods can become prohibitively expensive in terms of memory usage. The goal of this research is to: i) develop a fundamental relation based on the entropy potential; ii) create a data-driven model of entropy and its first and second-order derivatives, expressed as a function of density and internal energy; iii) test the performance of the data-driven thermodynamic model on a CFD case study. Notably, two Multi-Layer Perceptron (MLP) models are trained on a synthetic dataset comprising 500k thermodynamic state points, obtained by means of the Span-Wagner EoS. The thermodynamic properties are calculated by differentiating the fundamental equation, thus ensuring thermodynamic consistency. Conversely, thermodynamic stability is properly enforced during the regression process. Albeit the method is applicable to the development of equation of state models for arbitrary fluids and thermodynamic conditions, the present work only considers siloxane MM in the single phase region. The MLP model is implemented in the open-source SU2 software [8] and is used for the numerical simulation of non-ideal compressible flows in a planar converging-diverging nozzle. Finally, the accuracy and the computational performance of the data-driven thermodynamic model are assessed by comparing the resulting flow field, the wall time and the memory requirements with those obtained with direct calls to a cubic EoS, and with a LuT method.

Keywords: data-driven modeling · thermodynamic properties · computational fluid dynamics

1 Introduction

Flows of fluids not obeying to the perfect or the ideal gas law are encountered in many relevant engineering applications. In the field of propulsion and power, examples of these applications include unconventional turbines and compressors operating

M. White et al. (Eds.): NICFD 2022, ERCOFTAC 29, pp. 22–32, 2023.
https://doi.org/10.1007/978-3-031-30936-6_3

with dense vapors for power generation and thermal management systems [10], fuel injectors of gas turbines and regenerative cooling nozzles of rocket engines [1,2], in which the fluid is at supercritical conditions, and compact heat-exchangers for waste heat recovery systems, whereby the fluid can be either a non-ideal compressible liquid or a supercritical gas [4].

The accurate modeling of the thermodynamic properties of non-ideal fluid flows is usually obtained by resorting to multi-parameter equations of state (MEoS) in the Helmholtz free-energy form [5,21]. Models in this form for a variety of pure fluids and mixtures are implemented in popular thermodynamic software packages like RefProp [13], FluidProp [6], and CoolProp [3]. However, in the context of CFD, the computational overhead associated with direct calls to MEoS is typically excessive, especially if design optimization [19] or high-fidelity analyses [11,17] are involved.

Methods for the efficient calculation of thermodynamic properties can be divided in two classes: methods based on the interpolation of tabulated property values, commonly referred to as look-up table methods, and data-driven methods, in which thermodynamic models are constructed through a proper fitting of the fluid property values obtained with arbitrarily complex EoS. For instance, in [18], consistent thermodynamic models in the Helmholtz free-energy form satisfying the Maxwell relations were trained using an Artificial Neural Network (ANN), showing high-accuracy in the predicted fluid properties. Similarly, in [22], the authors compared the performance obtained by training a Multi-Layer Perceptron (MLP) and a Gaussian Process (GP) to replicate the statistical associating fluid theory (SAFT-VR) EoS for pure fluids, and concluded that the ANN outperforms the GP model.

For CFD simulations, LuT methods have been proven to be efficient and accurate, but data-driven methods provide advantages in terms of robustness and reduction of memory usage [12], thus making them particularly suitable for massively parallel computations. Longmire and Banuti [14,15] exploited tiny neural networks to compute the thermodynamic properties of CO_2 as a function of temperature, in the supercritical region. The objective was to perform viscous simulations of non-ideal flows in non-adiabatic laminary boundary layers, using the incompressible Navier-Stokes solver of SU2 [7]. Results show that the computational overhead while using the ANN model was about 20% higher compared to when using constant properties. In [16], the authors adopted an ANN to compute the thermodynamic and transport properties of multi-component mixtures for large-eddy simulations of turbulent mixing flows, and one-dimensional simulations of diffusive flames. As outcome of their study, the authors measured a speed-up of 1.5 and 2.3 times, respectively, compared to the baseline cases. Moreover, the authors stated that, for test cases involving many chemical species, the use of ANNs enables a reduction of memory usage of up to 5 orders of magnitude with respect to LuT methods. However, the data-driven regression technique described in the paper heavily relies on the injection of boundary information into the training dataset, making it application-specific. In addition, the average prediction errors for the primitive variables reported in the paper are in the range of 1–9%. This level of accuracy could lead to large discrepancies in the prediction of local flow phenomena involving large spatial gradients, e.g., shock-waves.

The objective of this work is the development of an accurate data-driven equation of state, tailored to compressible flow simulations of pure fluids and mixtures of fixed composition. The model is formulated in terms of entropy potential, i.e., $s = s(e, \rho)$. The desired level of accuracy and computational efficiency is attained by means of a semi-consistent formulation: a MLP model is trained on a dataset comprising 500k values of entropy and its first and second-order derivatives with respect to e and ρ, calculated with the Span-Wagner multi-parameter EoS implemented in [13]. It follows that, for a given thermodynamic state, s and its derivatives are computed with the MLP, while the primary and secondary thermodynamic properties are explicitly computed using their analytical definition based on the entropy potential. The semi-consistent MLP model has been implemented within the compressible Navier-Stokes solver of SU2 [8], and the resulting numerical model has been applied to perform simulations of non-ideal flows of siloxane MM in a converging-diverging nozzle.

2 Methodology

2.1 Fundamental Relation in Entropic Form

A thermodynamic model based on the entropy potential is highly suited for CFD applications featuring non-ideal flows, since its natural variables, i.e., e and ρ, are those used to retrieve the fluid properties in a flow solver. The proposed thermodynamic model is of general validity, i.e., it is applicable to any pure fluid and mixture of fixed composition, regardless of the thermodynamic state, both in the single and in the two-phase region. However, in the present work, its use is restricted to siloxane MM in the single phase region. Equations (1) to (4) provide the analytical expressions of the primary thermodynamic properties used by CFD compressible flow solvers, namely temperature, T, pressure, p, enthalpy, h, and speed of sound, c. Such relations have been derived from fundamental thermodynamic equations, by applying mathematical rules of multivariable differential calculus.

$$T = \left(\frac{\partial s}{\partial e}\right)_{\rho}^{-1} \quad (1) \qquad p = -\rho^2 \; T \left(\frac{\partial s}{\partial \rho}\right)_{e} \quad (2) \qquad h = e - \rho \left(\frac{\partial s}{\partial \rho}\right)_{e} \left(\frac{\partial s}{\partial e}\right)_{\rho}^{-1} \quad (3)$$

$$\begin{aligned} c^2 = \left(\frac{\partial p}{\partial \rho}\right)_{e} - \left(\frac{\partial p}{\partial e}\right)_{\rho} \left(\frac{\partial s}{\partial \rho}\right)_{e} \left(\frac{\partial s}{\partial e}\right)_{\rho}^{-1} = \\ - \rho \left(\frac{\partial s}{\partial e}\right)_{\rho}^{-1} \cdot \left\{ \left(\frac{\partial s}{\partial \rho}\right)_{e} \cdot \left[2 - \rho \left(\frac{\partial s}{\partial e}\right)_{\rho}^{-1} \cdot \left(\frac{\partial^2 s}{\partial \rho \partial e}\right) \right] + \rho \left(\frac{\partial^2 s}{\partial \rho^2}\right) + \\ - \rho \left[- \left(\frac{\partial s}{\partial e}\right)_{\rho}^{-1} \cdot \left(\frac{\partial^2 s}{\partial e^2}\right) \cdot \left(\frac{\partial s}{\partial \rho}\right)_{e} + \left(\frac{\partial^2 s}{\partial \rho \partial e}\right) \right] \cdot \left(\frac{\partial s}{\partial \rho}\right)_{e} \cdot \left(\frac{\partial s}{\partial e}\right)_{\rho}^{-1} \Bigg\} \end{aligned} \quad (4)$$

Secondary thermodynamic variables, which are needed to compute inviscid and viscous fluxes, and Jacobians, namely, $\left(\frac{\partial T}{\partial e}\right)_\rho$, $\left(\frac{\partial T}{\partial \rho}\right)_e$, $\left(\frac{\partial p}{\partial e}\right)_\rho$, $\left(\frac{\partial p}{\partial \rho}\right)_e$, are obtained by partial differentiation of Eqs. (1, 2), and are given by Eqs. (5) to (8).

$$\left(\frac{\partial T}{\partial e}\right)_\rho = -\left(\frac{\partial s}{\partial e}\right)_\rho^{-2} \cdot \left(\frac{\partial^2 s}{\partial e^2}\right) \quad (5) \qquad \left(\frac{\partial T}{\partial \rho}\right)_e = -\left(\frac{\partial s}{\partial e}\right)_\rho^{-2} \cdot \left(\frac{\partial^2 s}{\partial \rho \partial e}\right) \quad (6)$$

$$\left(\frac{\partial p}{\partial e}\right)_\rho = -\rho^2 \left(\frac{\partial s}{\partial e}\right)_\rho^{-1} \cdot \left\{-\left(\frac{\partial s}{\partial e}\right)_\rho^{-1} \cdot \left(\frac{\partial^2 s}{\partial e^2}\right) \cdot \left(\frac{\partial s}{\partial \rho}\right)_e + \left(\frac{\partial^2 s}{\partial \rho \partial e}\right)\right\} \quad (7)$$

$$\left(\frac{\partial p}{\partial \rho}\right)_e = -\rho \left(\frac{\partial s}{\partial e}\right)_\rho^{-1} \cdot \left\{\left(\frac{\partial s}{\partial \rho}\right)_e \cdot \left[2 - \rho \left(\frac{\partial s}{\partial e}\right)_\rho^{-1} \cdot \left(\frac{\partial^2 s}{\partial \rho \partial e}\right)\right] + \rho \left(\frac{\partial^2 s}{\partial \rho^2}\right)\right\} \quad (8)$$

Therefore, given the values of internal energy and density, all the necessary thermodynamic properties can be computed by resorting to the entropy potential and its first and second-order partial derivatives. Thermodynamic consistency is thus inherently guaranteed. Moreover, at each iteration of the flow solver, the thermodynamic state can be updated by means of explicit calculations, differently from what happens with other thermodynamic potentials, e.g., Helmholtz free energy, $a = a(T, \rho)$, for which the internal energy is retrieved by iteratively solving a non-linear equation.

The correctness of the analytical relations (4)–(8) has been assessed by comparing the thermodynamic property values obtained computing each right-hand side term of the equations through the CoolProp library [3] against those calculated by directly computing T, p, h, c^2, $\left(\frac{\partial T}{\partial e}\right)_\rho$, $\left(\frac{\partial T}{\partial \rho}\right)_e$, $\left(\frac{\partial p}{\partial e}\right)_\rho$, $\left(\frac{\partial p}{\partial \rho}\right)_e$ via direct EoS calls. For all properties, the deviations were, on average, in the order of $\mathcal{O}(10^{-13})$.

2.2 Data-Driven Modeling of Thermodynamic Properties

The development of the data-driven EoS model for the prescribed case study, i.e., siloxane MM in the vapor and supercritical regions, is documented in this section. A MLP, i.e., a feedforward ANN featuring one or multiple fully connected hidden layers, has been selected to accomplish this task. The reason is twofold. First, the computational overhead associated with the evaluation of the data-driven model is of primary importance for the target application. In general terms, the computational cost of a MLP model scales with the total number of neurons, and is lower than the cost of evaluating, for instance, a model based on a GP or a Support Vector Machine (SVM). On the other hand, an MLP model requires a larger amount of training data to reach the same level of accuracy of a GP or a SVM model. However, in the present work the dataset is synthetically generated by resorting to the MEoS implemented in [13], thus the availability of data is not a limiting factor.

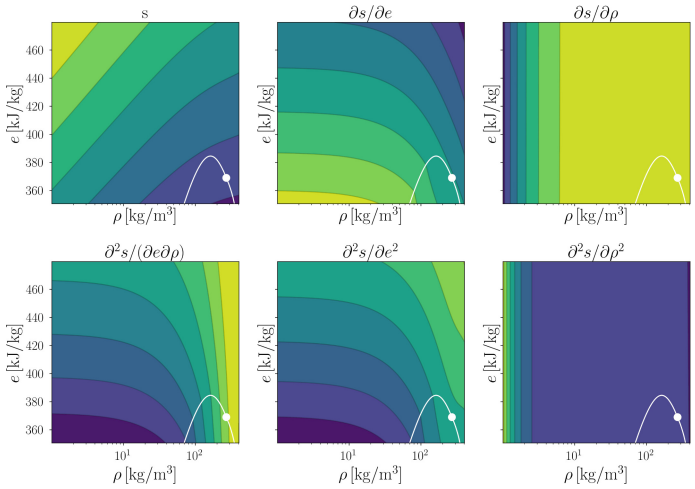

Fig. 1. Trends of the entropy potential, its first and its second-order derivatives with respect to density and internal energy. The white line identifies the saturation curve, while the white dot corresponds to the critical point. The range of density has been extended up to $405\ \mathrm{kg/m^3}$ for visualization purposes.

The ranges of variation of the input features, i.e., density and internal energy, selected to create the dataset are ρ = 1.0–295 $\mathrm{kgm^{-3}}$ and e = 350.6–479.8 $\mathrm{kJkg^{-1}}$, respectively. The trends of the labels, i.e., entropy potential and its first and second-order derivatives, are displayed in Fig. 1. Two observations can be drawn from such trends. On the one hand, the first and second-order partial derivatives of s with respect to ρ are characterized by large gradients at low values of density. As a result, training a MLP model over a wide range of density requires the use of a deeper network architecture, featuring a higher neuron count, thus an increased computational cost. To overcome this issue, while retaining a high level of accuracy, the dataset has been split in two parts, i.e., $\rho \leq 10\ \mathrm{kgm^{-3}}$, $\rho > 10\ \mathrm{kgm^{-3}}$, and a different MLP model has been trained over each portion of the dataset. On the other hand, the labels do not show large discontinuities across the saturation curve. As a consequence, training a MLP model over a dataset comprising both the single and the two-phase region should not involve additional complexity. Nevertheless, the development of data-driven EoS models for thermodynamic processes within the two-phase region is out of the scope of the present work.

As outcome of a sensitivity analysis, a dataset comprising 250k samples for each portion of the thermodynamic plane, i.e., $\rho \leq 10\ \mathrm{kgm^{-3}}$, $\rho > 10\ \mathrm{kgm^{-3}}$, has been selected as optimal trade-off between prediction accuracy and computational cost associated to training. To improve the performance of the MLP model, input features normalization and logarithmic transformation of the labels characterized by a highly skewed distribution, i.e., $\partial s/\partial \rho$ and $\partial^2 s/\partial \rho^2$, has been applied prior to training. Upon pre-processing, the dataset has been split into training, development, and test sets, counting 450k, 25k, and 25k samples, respectively.

In order to enhance the performance of the MLP models, a search for the optimal set of hyper-parameters was conducted by resorting to the latin-hypercube sampling, featuring 100 samples for each portion of the dataset. The design space comprises: the number of layers L, the number of neurons per layer $n^{[l]}$, the activation function, the learning rate α, and the mini-batch size. The performance of the different MLP architectures is measured in terms of computational cost at evaluation time $C(\Theta)$ and accuracy, i.e., loss $L(\Theta) = \frac{1}{n}\sum_{i=1}^{n}(\hat{y}_i - y_i)^2$ evaluated on the development set at the last epoch of training. The results are shown in Fig. 2. In the figures, the three different MLP architectures used for the CFD simulations are highlighted. The code used to train, test, and optimize the MLP architectures can be downloaded at[1].

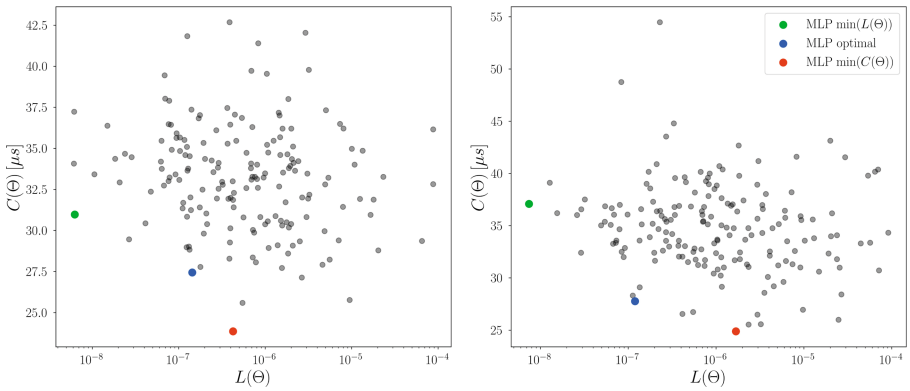

Fig. 2. Computational cost at evaluation time vs. loss evaluated on the development set for the MLP architectures selected for the hyper-parameters search. The results obtained for $\rho \leq 10\ \mathrm{kgm}^{-3}$ are shown on the left, while the performance of the MLPs trained over the portion of the dataset featuring $\rho > 10\ \mathrm{kgm}^{-3}$ are displayed on the right. The colored points highlight the MLP models selected for the CFD simulations.

Table 1. Set of hyper-parameters associated to the MLP architectures selected for the CFD analysis. For each hyper-parameter, the first entry corresponds to the model trained on the $\rho \leq 10\ \mathrm{kgm}^{-3}$ dataset, whereas the second entry refers to the model trained on the $\rho > 10\ \mathrm{kgm}^{-3}$ dataset.

Label	L	$n^{[1]}$	$n^{[2]}$	$n^{[3]}$	α	Activation	Mini-batch size
MLP optimal	2–2	90–19	16–51	0–0	$10^{-3.111}$–$10^{-4.019}$	swish - tanh	128–32
MLP $\min(C(\Theta))$	2–2	58–49	20–44	0–0	$10^{-4.737}$–$10^{-3.359}$	tanh - selu	32–512
MLP $\min(L(\Theta))$	3–3	90–29	50–70	9–66	$10^{-4.072}$–$10^{-3.844}$	sigmoid - gelu	32–16

3 Results

The computational performance of the MLP model was evaluated against direct calls to the MEoS implemented in [13]. The computational cost associated to the evaluation

[1] https://github.com/Propulsion-Power-TU-Delft/Deep.

of the thermodynamic state of siloxane MM on 250k samples of density and internal energy was measured for both the MLP model and the low-level C++ interface of CoolProp [3]. With reference to Fig. 2 and Table 1, the MLP architecture selected for this analysis was the MLP optimal. The benchmark has been performed on a workstation equipped with an 11th Gen Intel(R) Core(TM) i7-11700KF processor, featuring 8 cores and 16 threads, 32 GB of RAM, and a clock speed of 3.60 GHz. The evaluation of the entire dataset required 3.992×10^3 ms for the MLP, and 1.125×10^3 ms when resorting to the low-level interface of CoolProp. In other words, the data-driven model is approximately 2.8 times faster than the low-level interface of CoolProp.

3.1 CFD Analysis

In order to further assess the accuracy and the performance of the data-driven thermodynamic model, inviscid simulations of the supersonic flow within a planar De-Laval nozzle have been carried out. The converging-diverging nozzle has been designed to operate with siloxane MM as working fluid, at inlet conditions close to the critical point. At the inlet boundary, the total pressure and temperature have been set to $18.423\,\mathrm{bar}$ and 525 K, respectively. At the outlet boundary, a back-pressure equal to 10 bar has been prescribed, such to obtain a normal shock-wave in the diverging section of the nozzle. The computational domain, featuring 108k triangular elements, has been created with the unstructured mesh generator Gmsh [9]. To improve the resolution at the shock front and the convergence rate, local mesh refinement has been applied, by reducing the local cell size by a factor of 3. All simulations have been performed in two steps:

1. A maximum of 10k iterations using the ROE upwind scheme, featuring first-order spatial accuracy, and a Courant-Friedrichs-Lewy number (CFL) equal to 5;
2. A maximum of 30k iterations using the central scheme JST, featuring second and fourth order polynomial coefficients equal to 0.5 and 0.02, respectively, and a unitary CFL number.

Two different thermodynamic models have been used to verify the results obtained with the data-driven EoS: i) the polytropic Peng-Robinson (PPR) cubic EoS implemented in SU2; ii) an unstructured LuT method [20], resorting to a grid of about 250k thermodynamic state points, computed with the MEoS implemented in [13]. Figure 3 shows the contour of the Mach number obtained with the optimal MLP architecture, alongside with the relative percentage deviation computed with respect to the solution obtained with the LuT method. The maximum and minimum relative deviations are located at the shock-wave front, and are in the order of 5%, whereas the average relative deviations computed for the Mach, density, and pressure fields are 0.47%, 0.05%, and 0.03%, respectively. To further assess the discrepancy between the flow solutions computed with the different thermodynamic models, the Mach number at the nozzle center-line is displayed in Fig. 4. The excellent agreement between the Mach trend obtained with the MLP, the PPR and the LuT methods corroborate the validity of the novel data-driven thermodynamic model.

The ultimate goal of this study is to assess the suitability of data-driven thermodynamic models for massively parallel CFD calculations, both in terms of memory requirements and computational cost. To this purpose, the memory usage and

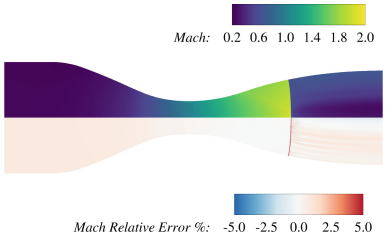

Fig. 3. Nozzle flow field. Upper half: Mach contours obtained with the optimal MLP architecture; Lower half: Mach number relative percentage deviation with respect to the *LuT* solution.

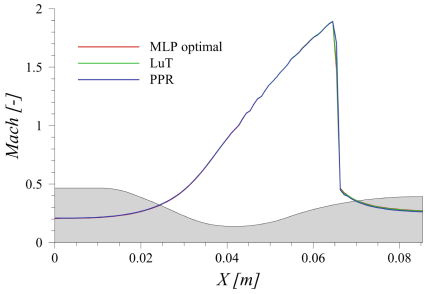

Fig. 4. Comparison of the Mach number trends computed along the nozzle center-line. The nozzle geometry is displayed in grey.

Table 2. Overview of the memory usage and the time/iteration obtained with the different fluid models.

Label	Memory [GB]	Time/Iteration [s]
LuT	9.0	2.754e−2
PPR	0.4	1.767e−2
MLP optimal	0.4	1.513e−1
MLP $\min(C(\Theta))$	0.4	1.882e−1
MLP $\min(L(\Theta))$	0.4	8.491e−1

the time per iteration of the flow solver have been recorded for each of the method described above. The benchmark provided in Table 2 has been conducted on a workstation equipped with an Intel(R) Xeon(R) Gold 5220R, featuring 24 cores, 48 threads, 256 GB of RAM, and a base and maximum clock speed of 2.2 and 4.0 GHz, respectively. The comparison shows a remarkable difference in terms of memory usage, with the data-driven model being comparable to the simpler cubic EoS, while the LuT method requires about 22.5 times more RAM. In terms of computational cost, the fastest of the MLP models is 5.5 times slower than the LuT method, and more than 8.5 times slower than the PPR. According to Fig. 2, the architecture labelled as MLP $\min(C(\Theta))$ should have provided the lowest computational cost. However, the model labelled as MLP optimal has been found to be the least computational intensive, when integrated within the flow solver. This discrepancy can be attributed to the sub-optimal implementation of the MLP model within SU2, as compared to the one featured in the state-of-the-art platform for machine learning that has been used to create such models, i.e., TensorFlow. The optimization of the MLP implementation within SU2 will be the objective of future research, with the purpose of reducing the computational overhead as compared to the LuT method.

The CFD simulations performed in this study have been run for a fixed number of iterations, so as to compare the convergence history obtained with the different fluid models. The normalized RMS values of the density and energy residuals is displayed in Fig. 5 for the optimal MLP, LuT and PPR test cases. When focusing on the initial 10k iterations, corresponding to the 1st order simulations, one can notice that the density residual of the PPR case drops by 5 orders of magnitude, whereas the decrease is limited to 3 orders of magnitude for the LuT and the MLP models. On the other hand, the trend of the energy residual is comparable for all the investigated fluid models. When examining the convergence history of the 2nd order simulations, i.e., the following 30k iterations, the LuT test case shows a reduction of the normalized residuals of 1.5 orders of magnitude, followed by an oscillatory trend. Conversely, both the PPR and the MLP cases are characterized by a smooth trend of the residuals. Such behavior is expected, since both fluid models are based on a continuous mathematical function, which does not involve any interpolation. As a result, the higher computational overhead associated with the MLP model can be partially compensated by its superior convergence properties, as compared to LuT methods.

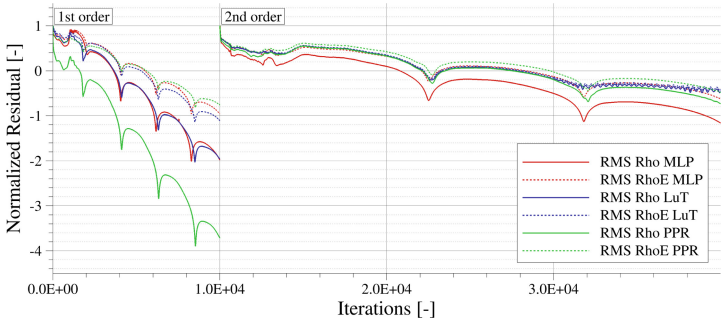

Fig. 5. Normalized density and energy residuals for the 1st and 2nd order simulations performed with the three investigated fluid models. The case featuring the PPR EoS reached the lowest absolute density residual.

4 Conclusions and Future Works

The research documented in this paper demonstrated that data-driven equations of state models based on the entropy potential are a valid alternative over look-up table (LuT) methods for non-ideal compressible flow simulations. Different artificial neural networks of the type of multi-layer perceptron (MLP) have been generated to compute the thermodynamic properties of siloxane MM in the vapor and supercritical region. The data-driven models have been implemented in the open-source SU2 software to perform a simulation of a shock-induced non-ideal flow within a planar converging-diverging nozzle. Comparisons between simulation results obtained with the MLP and with the LuT and a polytropic Peng-Robinson model have been made in terms of accuracy and computational performance. Results computed with MLP and LuT are

in excellent quantitative agreement, but the CFD simulations carried out with the LuT are approximately 5 times faster than those run with the MLP. Conversely, the use of the MLP is 20 times less memory intensive, and shows better convergence properties. Future work will target the optimization of the MLP implementation within the flow solver of SU2 for massively parallel computations of non-ideal compressible flows in turbomachinery applications.

References

1. Banuti, D.: Why we need to care about supercritical and non-ideal injection. In: APS Division of Fluid Dynamics Meeting Abstracts, p. T01.008, AA. University of New Mexico, January 2021
2. Banuti, D.T.: A thermodynamic look at injection in aerospace propulsion systems. In: AIAA Scitech 2020 Forum, Number 0 in AIAA SciTech Forum. American Institute of Aeronautics and Astronautics, 15 July 2022
3. Bell, I.H., Wronski, J., Quoilin, S., Lemort, V.: Pure and pseudo-pure fluid thermophysical property evaluation and the open-source thermophysical property library CoolProp. Ind. Eng. Chem. Res. **53**(6), 2498–2508 (2014)
4. Brun, K., Friedman, P., Dennis, R.: Fundamentals and Applications of Supercritical Carbon Dioxide (sCO_2) Based Power Cycles. Woodhead Publishing (2017)
5. Colonna, P., Nannan, N.R., Guardone, A., Lemmon, E.W.: Multiparameter equations of state for selected siloxanes. Fluid Phase Equilib. **244**(2), 193–211 (2006)
6. Colonna, P., van der Stelt, T.P., Guardone, A.: FluidProp (version 3.0): a program for the estimation of thermophysical properties of fluids. Asimptote, Delft, The Netherlands (2012). http://www.fluidprop.com
7. Economon, T.D.: Simulation and adjoint-based design for variable density incompressible flows with heat transfer. AIAA J. **58**(2), 757–769 (2022)
8. Economon, T.D., Palacios, F., Copeland, S.R., Lukaczyk, T.W., Alonso, J.J.: SU2: an open-source suite for multiphysics simulation and design. AIAA J. **54**(3), 828–846 (2015). https://doi.org/10.2514/1.J053813
9. Geuzaine, C., Remacle, J.F.: Gmsh: a 3-D finite element mesh generator with built-in pre- and post-processing facilities. Int. J. Numer. Methods Eng. **79**(11), 1309–1331 (2009)
10. Giuffre, A., Colonna, P., Pini, M.: The effect of size and working fluid on the multi-objective design of high-speed centrifugal compressors. Int. J. Refrig **143**, 43–56 (2022)
11. Hoarau, J.-C., Cinnella, P., Gloerfelt, X.: Large eddy simulations of strongly non-ideal compressible flows through a transonic cascade. Energies **14**(3), 772 (2021)
12. Ihme, M., Schmitt, C., Pitsch, H.: Optimal artificial neural networks and tabulation methods for chemistry representation in LES of a bluff-body swirl-stabilized flame. Proc. Combust. Inst. **32**(1), 1527–1535 (2009)
13. Lemmon, E.W., Bell, I.H., Huber, M.L., McLinden, M.O.: NIST standard reference database 23: reference fluid thermodynamic and transport properties-REFPROP, version 10.0. National Institute of Standards and Technology (2018)
14. Longmire, N., Banuti, D.T.: Onset of heat transfer deterioration caused by pseudo-boiling in CO_2 laminar boundary layers. Int. J. Heat Mass Transf. **193**, 122957 (2022)
15. Longmire, N.P., Banuti, D.: Extension of SU2 using neural networks for thermo-fluids modeling. In: AIAA Propulsion and Energy 2021 Forum, Number 0 in AIAA Propulsion and Energy Forum. American Institute of Aeronautics and Astronautics, 10 July 2022
16. Milan, P.J., Hickey, J.-P., Wang, X., Yang, V.: Deep-learning accelerated calculation of real-fluid properties in numerical simulation of complex flowfields. J. Comput. Phys. **444**, 110567 (2021)

17. Przytarski, P.J., Wheeler, A.P.S.: Accurate prediction of loss using high fidelity methods. J. Turbomach. **143**(3), 031008 (2022)
18. Rosenberger, D., Barros, K., Germann, T.C., Lubbers, N.: Machine learning of consistent thermodynamic models using automatic differentiation. Phys. Rev. E **105**(4), 045301 (2022)
19. Rubino, A., Colonna, P., Pini, M.: Adjoint-based unsteady optimization of turbomachinery operating with nonideal compressible flows. J. Propul. Power **37**(6), 910–918 (2022)
20. Rubino, A., Pini, M., Kosec, M., Vitale, S., Colonna, P.: A look-up table method based on unstructured grids and its application to non-ideal compressible fluid dynamic simulations. J. Comput. Sci. **28**, 70–77 (2018)
21. Span, R., Wagner, W.: Equations of state for technical applications. II. Results for nonpolar fluids. Int. J. Thermophys. **24**(1), 41–109 (2003). https://doi.org/10.1023/A:1022310214958
22. Zhu, K., Müller, E.A.: Generating a machine-learned equation of state for fluid properties. J. Phys. Chem. B **124**(39), 8628–8639 (2020)